PRAMANA — journal of physics



Vol. 82, No. 4
April 2014
pp. 727–741

# The effect of nuclear structure in the emission of reaction products in heavy-ion reactions

SAMIR KUNDU

Variable Energy Cyclotron Centre, 1/AF, Bidhan Nagar, Kolkata 700 064, India
E-mail: skundu@vecc.gov.in; samir.kundu@gmail.com

**DOI:** 10.1007/s12043-014-0724-7; ***e*Publication:** 5 April 2014

**Abstract.** Study of intermediate mass fragments (IMFs) and light charged particles (LCPs) emission has been carried out for a few reactions involving $\alpha$-cluster and non-$\alpha$-cluster systems to see how the emission processes are affected by nuclear clustering. Li, Be, B and $\alpha$-particles have been studied from $\alpha$-clustered system $^{16}O + {}^{12}C$ for 117, 125, 145 and 160 MeV bombarding energies respectively. The enhanced yields of near-entrance channel fragment B and large quadrupole deformation of the produced composite $^{28}Si^*$ extracted from LCP spectra indicate the survival of orbiting-like process in $^{16}O + {}^{12}C$ system at these energies. The same IMFs emitted from the $\alpha$-cluster system $^{12}C$ (77 MeV) + $^{28}Si$ and nearby non-$\alpha$ cluster $^{11}B$ (64 MeV) + $^{28}Si$ and $^{12}C$ (73 MeV) + $^{27}Al$ (all having the same excitation energy of $\sim$67 MeV) have also been studied. The fully energy damped (fusion–fission) and the partially energy damped (deep inelastic) components of the fragment energy spectra have been extracted. It has been found that the yields of the fully energy damped fragments for all the above reactions are in conformity with the respective statistical model predictions. The time-scales of various deep inelastic fragment emissions have been extracted from the angular distribution data. The angular momentum dissipation in deep inelastic collisions has been estimated from the data and it has been found to be close to the corresponding sticking limit value.

**Keywords.** Fusion–fission reactions; statistical model; strongly damped collisions; compound nucleus; dinuclear orbiting; deformation.

**PACS Nos 25.70.Jj; 24.60.Dr; 25.70.Lm; 25.70.Gh; 27.30.+t**

## 1. Introduction

Exploring the role of clustering of the colliding light heavy-ions in the emission of intermediate mass fragment, light charged particle and fusion–fission (FF) is one of the active subject in low-energy nuclear reactions. Extensive studies have been done to understand the fragment emission mechanisms in low-energy ($E_{\text{lab}} \leq 10$ MeV/u) light heavy-ion ($A_{\text{proj.}} + A_{\text{tar.}} \lesssim 60$) reactions [1–3]. Most of the studies show that the fragments are

emitted from quasielastic (QE)/projectile breakup [4], deep inelastic (DI) transfer and FF [5] processes. But, in some cases the structure of the nuclei has been found to play an important role. In the reactions involving $\alpha$-cluster nuclei (e.g., $^{20}$Ne + $^{12}$C [6], $^{24}$Mg + $^{12}$C [7], $^{28}$Si + $^{12}$C [8] etc.) where the observations of large enhancement in yield and/or resonance-like excitation function in a few outgoing channels (near to the entrance channel) have indicated the competitive role played by the deep inelastic orbiting (DIO) mechanism [6].

Deep inelastic orbiting is described in terms of the formation of a long-lived, dinuclear molecular complex [9], with a strong memory of the entrance channel. In addition, in the case of the light heavy-ion systems, the shapes of the orbiting dinuclear complexes are quite similar to the saddle and scission shapes obtained in the course of evolution of the FF process. Both orbiting and fusion–fission processes occur on similar time-scales and hence, the distinction between the signatures of the two processes is a real challenge. But there are some special features in case of dinuclear orbiting. The orbiting and resonance contributions of the reaction yields occur because of the weak absorption of the partial waves near grazing angular momentum. This 'surface transparency' may be related to the number of open reaction channels (NOC) in lighter systems [10]. In light heavy-ion systems a strong correlation has been observed between the existence of very low NOC and the occurrence of resonant behaviour and back-angle enhancement in the elastic, inelastic, or transfer channels [11]. It is also found that in orbiting dinuclear systems, deformation in the produced composite, is also very large. Detailed study of the deformation of $^{40}$Ca$^*$ [12] and $^{32}$S$^*$ [13] was done recently with the help of light charged particle (LCP) spectroscopy to extract 'anomalous' deformation in these cases confirming the presence of DIO mechanism. For these systems, orbiting ($^{40}$Ca$^*$ [14], $^{32}$S$^*$ [6]) had already been conjectured from the fragment emission studies.

In this study, two experiments have been performed. In the first experiment [15,16], the reaction mechanism of IMF emission and its evolution with bombarding energy have been studied in the $\alpha$-cluster system $^{16}$O+$^{12}$C [15]. Quadrupole deformation parameter of the composite system ($^{28}$Si$^*$) has been estimated by comparing slopes of the LCP spectra with the same obtained from statistical model predictions [16]. In the second experiment [17], the emission processes of IMF have been studied in the $\alpha$-cluster system $^{12}$C + $^{28}$Si and the neighbouring non-$\alpha$-cluster systems $^{11}$B + $^{28}$Si and $^{12}$C + $^{27}$Al, all having the same excitation energy ($\sim$ 67 MeV), in order to look into the roles played by various IMF emission processes in these reactions.

## 2. Experiment

The first experiment [15,16] was performed at the Variable Energy Cyclotron Centre, Kolkata, using $^{16}$O ion beams of energies of 117, 125, 145 and 160 MeV, respectively. The target used was $\sim$514 $\mu$g/cm$^2$ self-supporting $^{12}$C. Different fragments were detected using two Si(SB) telescopes ($\sim$10 $\mu$m $\Delta E$, $\sim$300 $\mu$m $E$ and $\sim$10 $\mu$m $\Delta E$, $\sim$5 mm $E$). Inclusive energy distributions for the various fragments ($3 \leq Z \leq 5$) and $\alpha$-particles have been measured in the angular range 9–29°. The second experiment [17] was performed using $^{12}$C and $^{11}$B ion beams from the BARC-TIFR 14UD Pelletron accelerator at Mumbai. The $^{12}$C ion beam of 77 MeV energy was bombarded on a self-supporting $^{28}$Si target

of thickness ∼1 mg/cm$^2$, to produce $^{40}$Ca$^*$ at ∼67 MeV of excitation energy. In addition, the $^{12}$C ion beam of 73 MeV energy and the $^{11}$B ion beam of 64 MeV energy were bombarded on $^{27}$Al (self-supporting, ∼500 $\mu$g/cm$^2$), $^{28}$Si (thickness same as above) targets, respectively, to produce the same composite $^{39}$K$^*$, at the same excitation energy (∼67 MeV). The fragments ($3 \leq Z \leq 5$) have been detected using silicon detector (SB) telescopes (∼10 $\mu$m $\Delta E$, ∼350 $\mu$m $E$). The inclusive energy distributions of the emitted fragments (Li, Be, B) for each reaction have been measured in the laboratory angular range of ∼12–55°.

## 3. Results

### 3.1 *Energy spectra*

The energy spectra for the fragments B, Be and Li obtained from reaction $^{16}$O + $^{12}$C are shown in figure 1. It is observed that the energy spectra are typically Gaussian in shape and their centroids correspond to the expected kinetic energies for the binary breakup obtained from the Viola systematics corrected by the corresponding asymmetric factors [18]. The Gaussian fit [15] so obtained are shown by solid lines in figure 1 with centroids shown by solid arrows. In the case of B, there is significant enhancement in yield at the lower energy part of the spectrum which increases with bombarding energy. The width of the Gaussian distributions were extracted by constructing the fit to higher energy part of the spectrum (above the centroid energy), to minimize the contamination from enhanced

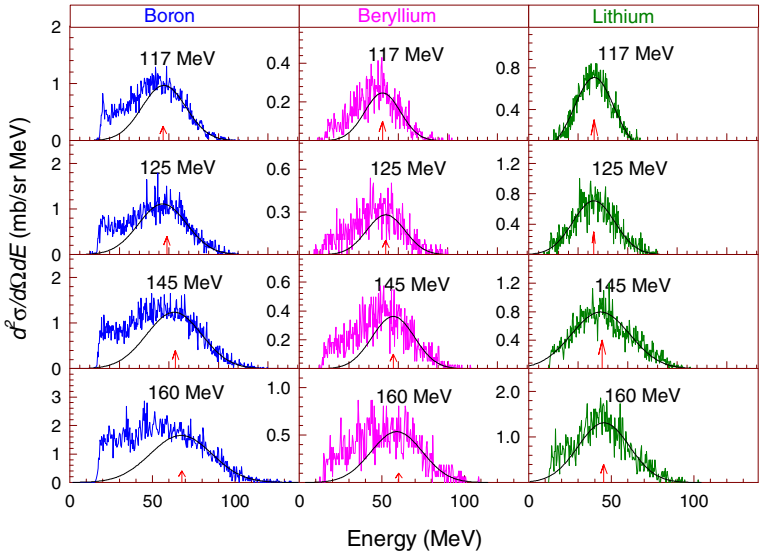


**Figure 1.** Typical energy spectra of fragments (B, Be and Li) emitted in the reaction $^{16}$O + $^{12}$C detected at an angle $\theta_{\rm lab} = 15°$ at respective $E_{\rm lab}$. Arrows indicate the centroid of the Gaussian distributions.

low-energy part of the spectrum. The explanation of enhanced yields at lower energy part of the spectrum is given in detail in the following section. The centre-of-mass energy spectra of the $\alpha$-particles emitted in the reactions $^{16}O + {}^{12}C$ at different beam energies are shown in figure 2. The slopes of the energy spectra measured at the lowest angle are compared with the same at highest angles and it is found that slopes are same. So, it may be concluded that the effects of other direct reaction mechanisms are not significant at the measured angles [16].

Typical energy spectra of the fragments ($3 \leq Z \leq 5$) emitted in $^{11}B$ (64 MeV) + $^{28}Si$, $^{12}C$ (73 MeV) + $^{27}Al$ and $^{12}C$ (77 MeV) + $^{28}Si$ reactions are shown in figure 3. The shapes of the fragment energy spectra obtained in the three reactions are quite different, because of the variation of relative contributions of different reaction processes in each case. It is found that the energy distributions of all the fragments have two peaks. To separate out fragments coming from different processes, each of these peaks is fitted with separate Gaussian functions as prescribed in [3]. The first peak position nearly matches with the energy obtained from Viola systematics, duly corrected for the asymmetric factor [18]. So, it may be assumed that the first peak comes from the FF process. The FF component of the energy spectrum thus obtained has then been subtracted from the full energy spectrum. This subtracted spectrum has been fitted with a second Gaussian, which was found to be originated from DI process as discussed in the following sections. The contributions of FF and DI components thus obtained (for each fragment) are displayed in figure 3. In each spectrum, the arrow at lower (higher) energy indicates the position of the centroid of the FF (DI) energy distribution.

### 3.2 *Angular distributions*

The differential cross-sections for fragments B, Be and Li have been obtained by integrating the respective energy distributions under the fitted Gaussian (first Gaussian for the FF

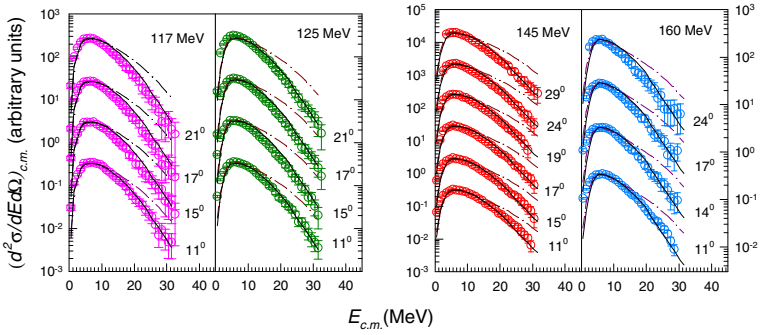


**Figure 2.** Energy spectra (c.m.) of $\alpha$-particles obtained at different angles for different beam energies for the reaction $^{16}O + {}^{12}C$. The symbols represent experimental data. The dash–dot–dashed and solid lines represent CASCADE calculations with RLDM and optimized values of spin-dependent 'deformability' parameters, respectively (see table 1). All experimental and calculated spectra, starting from the lowest angle, were multiplied by $10^{-2}$, $10^{-1}$, $10^{0}$, $10^{1}$, $10^{2}$, $10^{3}$, respectively.

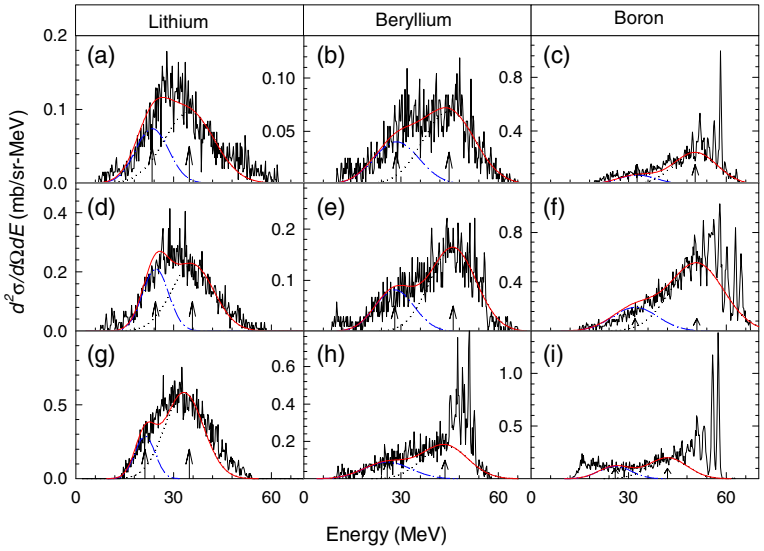


**Figure 3.** Typical energy spectra of the fragments measured for the reactions $^{12}C + ^{28}Si$ (**a**)–(**c**), $^{12}C + ^{27}Al$ (**d**)–(**f**) and $^{11}B + ^{28}$ Si (**g**)–(**i**) at $\theta_{lab} = 17.5°$ (**a**)–(**h**) and 30° (**i**). The blue dash–dotted, the black dotted and the red solid curves represent the contributions of the FF, the DI, and the sum (FF + DI), respectively. The left and the right arrows correspond to the centroids of FF and DI components of energy distributions, respectively.

fragment in the second experiment). The angular distribution of the fragments B, Be and Li obtained at all bombarding energies are found to follow $\sim 1/\sin\theta_{c.m.}$ dependence in c.m. frame which is characteristic of the fission-like decay of an equilibrated composite system [15,17]. The DI component of the fragment angular distribution has been obtained by integrating the respective Gaussian extracted from the energy distribution data. The c.m. angular distributions of DI components $d\sigma/d\Omega_{DI}$ of the fragments are displayed in figure 4. It is found that they fall much faster than $\sim 1/\sin\theta_{c.m.}$ distribution, indicating shorter lifetime of the composite system. It is possible to estimate the lifetime of

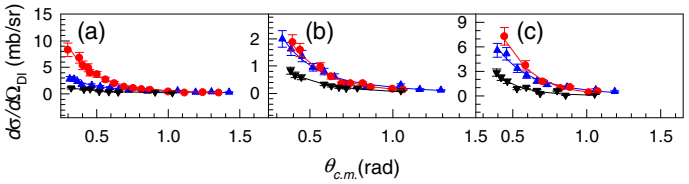


**Figure 4.** The c.m. angular distributions of the DI fragments [Li (**a**), Be (**b**) and B (**c**)]. The solid circles (red), triangles (blue) and inverted triangles (black) correspond to the experimental data for $^{11}B + ^{28}Si$, $^{12}C + ^{27}Al$ and $^{12}C + ^{28}Si$ reactions, respectively; the solid lines are the fits to the data (see text).

the intermediate dinuclear complex using a diffractive Regge-pole model [19] from these measured forward peaked angular distributions by fitting it with the following expression:

$$\left(\frac{\mathrm{d}\sigma}{\mathrm{d}\Omega}\right)_{\mathrm{DI}} = \left(\frac{C}{\sin\theta_{\mathrm{c.m.}}}\right)(\mathrm{e}^{-\theta_{\mathrm{c.m.}}/\omega\tau_{\mathrm{DI}}}). \tag{1}$$

The expression describes the decay of a dinucleus rotating with an angular velocity $\omega = \hbar\ell/\mu R^2$, where $\mu$ is the reduced mass of the system, $\ell$ the angular momentum ($\ell_{\mathrm{cr}} < \ell < \ell_{\mathrm{gr}}$; $\ell_{\mathrm{gr}}$, $\ell_{\mathrm{cr}}$ being the grazing and the critical angular momenta, respectively), $R$ represents the distance between the two centres of the dinucleus and $\tau_{\mathrm{DI}}$ is the time interval during which the two nuclei remain in a solid contact in the form of the rotating dinucleus. The value of the 'life angle' $\alpha(=\omega\tau_{\mathrm{DI}})$ decides the time-scale of the reaction. The time-scales for different DI fragments (Li, Be and B) thus obtained are shown in figure 5 for comparison. It is seen that, in all reactions, the time-scale decreases as the fragment charge increases, which is in conformity with a previous study by Mikumo *et al* [19]. The c.m. angular distributions, $(\mathrm{d}\sigma/\mathrm{d}\theta)_{\mathrm{c.m.}}$ of $\alpha$-particles emitted in the reaction $^{16}\mathrm{O} + {}^{12}\mathrm{C}$, obtained by integrating the c.m. energy distributions for the beam energies of 117, 125, 145 and 160 MeV, are found to be constant over the whole range of observed c.m. angles, which is characteristic of the emission from an equilibrated composite nucleus.

### 3.3 *Angular distribution of average Q-value of the IMFs*

The average $Q$-values, $\langle Q\rangle$, for all the fragments emitted in the reaction $^{16}\mathrm{O} + {}^{12}\mathrm{C}$ are calculated at all measured angles and found to be nearly constant. The independence of $\langle Q\rangle$ with respect to the emission angle suggests that, the fragments are emitted from a complete energy equilibrated system at all beam energies. Similar results have also been observed in the case of FF fragments emitted in the reactions $^{12}\mathrm{C} + {}^{28}\mathrm{Si}$, $^{11}\mathrm{B} + {}^{28}\mathrm{Si}$ and $^{12}\mathrm{C} + {}^{27}\mathrm{Al}$. The average $Q$ values ($\langle Q_{\mathrm{DI}}\rangle$) of the DI fragments emitted from $^{12}\mathrm{C} + {}^{28}\mathrm{Si}$, $^{11}\mathrm{B} + {}^{28}\mathrm{Si}$ and $^{12}\mathrm{C} + {}^{27}\mathrm{Al}$, estimated from the fragment kinetic energies assuming two-body kinematics, are displayed in figure 6 as a function of the c.m. angle. It is found that, for all fragments, the $\langle Q_{\mathrm{DI}}\rangle$ values tend to decrease with the increase of angles for $\theta_{\mathrm{c.m.}} \lesssim 40°$, and then gradually become nearly constant. It implies that, beyond this point, the kinetic energy damping is complete and dynamic equilibrium has been established before the scission of the dinuclear composite takes place.

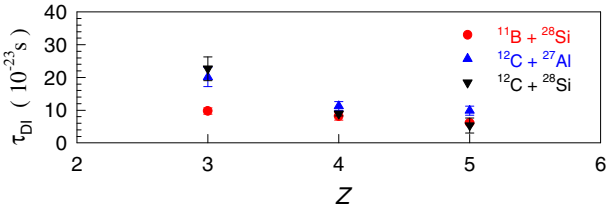


**Figure 5.** The emission time-scales of different DI fragments.

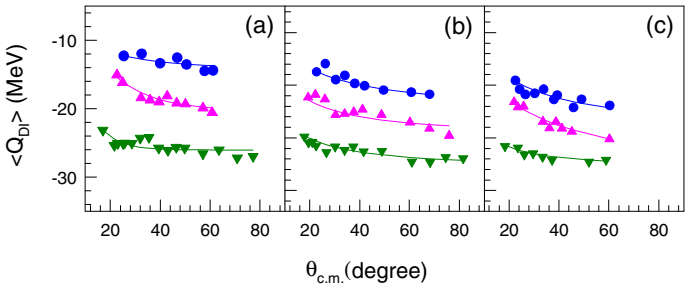


**Figure 6.** The average $Q$ values, $\langle Q_{\mathrm{DI}} \rangle$, plotted as a function of $\theta_{\mathrm{c.m.}}$ for Li (green inverted triangle), Be (pink triangle) and B (blue solid circle) emitted in (**a**) $^{11}\mathrm{B} + {}^{28}\mathrm{Si}$, (**b**) $^{12}\mathrm{C} + {}^{27}\mathrm{Al}$ and (**c**) $^{12}\mathrm{C} + {}^{28}\mathrm{Si}$ reactions. Solid lines are plotted to guide the eye.

### 3.4 *Average velocity of α-particles*

The average velocities, $v_{\mathrm{av}}$, of the $\alpha$-particles emitted at different angles have been extracted from the average energy. The parallel ($v_{||}$) and perpendicular ($v_{\perp}$) components (with respect to the beam direction) of $v_{\mathrm{av}}$ at each angle are plotted in figure 7. It is seen that they fall on a circle with the centre at CN velocity, $v_{\mathrm{CN}}$, and radius of average velocity in c.m., $v_{\mathrm{av}}^{\mathrm{c.m.}}$, which implies that the average velocities (as well as energies) of the $\alpha$-particles are independent of the c.m. emission angles. It again indicates that the $\alpha$-particles are emitted from a fully energy equilibrated source moving with the velocity $v_{\mathrm{CN}}$.

### 3.5 *Total cross-section of IMFs*

All these above observations show that the fragments coming from reactions $^{16}\mathrm{O} + {}^{12}\mathrm{C}$, $^{11}\mathrm{B} + {}^{28}\mathrm{Si}$, $^{12}\mathrm{C} + {}^{27}\mathrm{Al}$ and $^{12}\mathrm{C} + {}^{28}\mathrm{Si}$ (fragments under first peak of the energy spectra for the last three reactions) have been emitted either from a fully equilibrated CN, or, from a long-lived orbiting dinuclear system, or, from both. It may be noted here that, in dinuclear orbiting, the composite system is fully energy equilibrated but shape is not equilibrated. To get further information about the emission process, the angle-integrated fragment yields obtained from the fitted Gaussians, have been compared with the

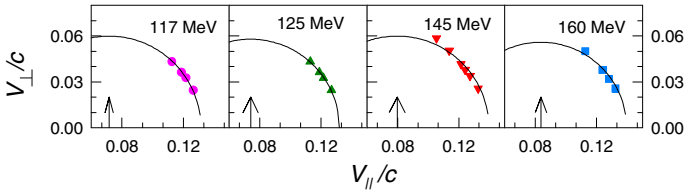


**Figure 7.** Average velocity curve of the $\alpha$-particles emitted in the reaction $^{16}\mathrm{O} + {}^{12}\mathrm{C}$. Symbols correspond to experimental data and solid lines show fit to the data obtained using the equation $v_{\perp}^2 = (v_{\mathrm{av}}^{\mathrm{c.m.}})^2 - (v_{||} - v_{\mathrm{CN}})^2$, where $v_{\mathrm{av}}^{\mathrm{c.m.}}$ is the average velocity of $\alpha$-particles in the c.m. frame. The arrow indicates the position of $v_{\mathrm{CN}}$.

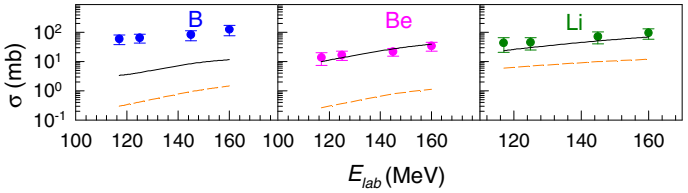


**Figure 8.** Excitation functions for the angle-integrated (over the range $0^\circ \leq \theta_{\mathrm{c.m}} \leq 180^\circ$) cross-section of the B, Be and Li fragments. Solid curves are the predictions of the statistical model with angular momentum $\ell = \ell_{\mathrm{cr}}$. Short dashed curves are the prediction from EHFM.

theoretical predictions of the standard statistical model codes, i.e., CASCADE [20] and extended Hauser–Feshbach model (EHFM) [21]. The experimental yields of IMFs emitted in the $^{16}$O + $^{12}$C reaction for different incident energies are shown in figure 8 by symbols. The solid lines are the same obtained from CASCADE with angular momentum up to $\ell_{\mathrm{cr}}$, the critical angular momentum of fusion. The values of $\ell_{\mathrm{cr}} = 20, 21, 22$ and $23\hbar$ [22] for 117, 125, 145 and 160 MeV beam energy, respectively. It has been observed that the CASCADE prediction matches well with the experimental yields of the fragments Li and Be. But it underpredicts the B yield. In the case of EHFM, the predicted yields are less than the measured yields for all fragments under study, as shown by dashed line in figure 8. The experimental angle-integrated yields of the FF fragments for all the three reactions under the second experiment are shown in figure 9. It is found that the yields of Li and Be in $^{11}$B + $^{28}$Si and $^{12}$C + $^{27}$Al reactions are nearly the same; the absence of any entrance channel dependence confirms their compound nuclear origin. It has also been observed that the yields of these fragments are comparable to those obtained in $^{12}$C + $^{28}$Si reaction. The yield of B in the $^{11}$B + $^{28}$Si reaction has been found to be slightly more than that obtained in the other two reactions, which might be due to the contamination from the beam-like channels in the former case, where B was the projectile. The experimental FF fragment yields have been compared with the theoretical estimates of the

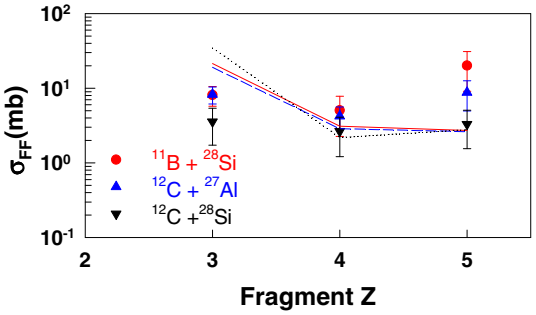


**Figure 9.** The total FF fragment cross-sections for the three reactions. The solid circles (red), triangles (blue) and inverted triangles (black) correspond to the experimental data for $^{11}$B + $^{28}$Si, $^{12}$C + $^{27}$Al and $^{12}$C + $^{28}$Si reactions, respectively. The solid (red), dashed (blue) and dotted (black) lines are the corresponding theoretical predictions.

same obtained from the extended Hauser–Feshbach model [21]. The values of the critical angular momentum, $\ell_{cr}$, for all the three systems, have been the same ($27\hbar$) [12,22,23]. The calculated fragment emission cross-sections are shown in figure 9. It is seen from the figure that in all three cases, the theoretical predictions are nearly the same and are in fair agreement with the experimental results.

### 3.6 *Energy spectra of α-particles and statistical model calculation*

The measured energy spectra of $\alpha$-particles emitted in the reaction $^{16}O + {}^{12}C$ have been compared with the respective normal CASCADE calculations which are shown in figure 2 by dash–dot–dash line. Details of the input parameters may be found in [16]. The value of the 'deformability parameters', $\delta_1$ and $\delta_2$ has been predicted (see $\delta_1^A$ and $\delta_2^A$ in table 1) by rotating liquid drop model (RLDM) [24]. It is clear from figure 2 that normal CASCADE calculation failed to reproduce the higher energy part of the energy spectra. The standard form of CASCADE is quite successful in explaining the LCP evaporation in the light ion-induced reaction in general, where the CN is assumed to be nearly spherical. However, in the case of heavy-ion-induced reaction, there is appreciable deviation between the experimental and the predicted LCP evaporation spectra. This deviation is attributed to the deformation of the excited compound system which is angular momentum-dependent. The deformation affects the particle spectra in two ways. First, it lowers the effective emission barrier, and second, it increases the moment of inertia. The first effect modifies the transmission coefficients for the evaporated particles which may be taken care of by increasing the radius parameter of optical model potential. However, the change in moment of inertia affects the level density and the slope of the higher energy part of the particle spectrum. This can be taken care of by incorporating the spin-dependent deformability parameters [25] in the expression of level density [16]. The effective moment of inertia, $\mathscr{I}_{\text{eff}}$ with deformability parameters, is written as

$$\mathscr{I}_{\text{eff}} = \mathscr{I}_0(1 + \delta_1\ell^2 + \delta_2\ell^4), \tag{2}$$

where $\mathscr{I}_0$ ($= \frac{2}{5}A^{5/3}r_0^2$) is the rigid-body moment of inertia, $\delta_1$ and $\delta_2$ are the deformability parameters, $r_0$ is the radius parameter. We have chosen $r_0 = 1.29$ which reproduced the lower energy part of the spectra. A similar value was used in [26]. The level density parameter $a$ was taken to be $A/8$ as in [25,27]. To reproduce the present experimental spectra, we have only changed the deformability parameters $\delta_1$ and $\delta_2$, as in [25]. To

**Table 1.** The values of different sets of 'deformability' parameters: $A$ – obtained from RLDM and $B$ – obtained by fitting the experimental data (see text). $E_{\text{lab}}$, $E$, $\ell_{cr}$ and $\ell_{av}$ are the beam energy, excitation energy, critical angular momentum and average angular momentum, respectively.

| $E_{\text{lab}}$ | $E$ | $\ell_{cr}$ | $\ell_{av}$ | $\delta_1^A$ | $\delta_2^A$ | $\delta_1^B$ | $\delta_2^B$ |
|---|---|---|---|---|---|---|---|
| 117 | 67 | 20 | 13 | $3.7 \times 10^{-4}$ | $1.1 \times 10^{-6}$ | $1.9 \times 10^{-3}$ | $2.0 \times 10^{-8}$ |
| 125 | 70 | 21 | 14 | $3.7 \times 10^{-4}$ | $1.1 \times 10^{-6}$ | $2.1 \times 10^{-3}$ | $2.0 \times 10^{-8}$ |
| 145 | 79 | 22 | 15 | $3.7 \times 10^{-4}$ | $1.1 \times 10^{-6}$ | $2.3 \times 10^{-3}$ | $2.0 \times 10^{-8}$ |
| 160 | 85 | 23 | 15 | $3.7 \times 10^{-4}$ | $1.1 \times 10^{-6}$ | $2.5 \times 10^{-3}$ | $2.0 \times 10^{-8}$ |

reproduce the whole spectra, we have followed the procedure proposed by Huizenga *et al* [25]. The deformability parameters $\delta_1$ and $\delta_2$ have been suitably optimized to reproduce the experimental spectra, which in effect modified the phase-space for statistical decay by relocation of the yrast line. The results with these modified deformability parameters are shown by solid lines in figure 2 and the optimized values of deformability parameters, $\delta_1^B$ and $\delta_2^B$, are given in table 1.

### 3.7 *Quadrupole deformation calculation*

The deformation of the excited composite may be expressed in terms of the standard quadrupole deformation parameter, $\beta$, using the procedure given in [28]. It was assumed that the shapes of the non-deformed and the deformed nuclei are spherical and symmetric ellipsoid in shape with volume $\frac{4}{3}\pi R_0^3$ and $\frac{4}{3}\pi abc$, respectively, where $R_0$ is the radius of the non-deformed nucleus and $a$, $b$, $c$ are the three semi-axis of the ellipsoid with sharp surfaces [25]. The effective moment of inertia can be expressed as

$$\mathscr{I}_{\text{eff}} = \frac{2}{5} M R_{\text{eff}}^2 = \frac{1}{5} M(a^2 + b^2), \tag{3}$$

where $c$ is the axis of rotation. In case of prolate shape, $a = c$ and $b$ ($>a$, $c$) is the symmetry axis. So, from eqs (2) and (3), one obtains

$$R_{\text{eff}}^2 = R_0^2(1 + \delta_1 \ell^2 + \delta_2 \ell^4) = \frac{1}{2}(a^2 + b^2). \tag{4}$$

Using eqs (3) and (4) along with the criterion of volume conserving deformation ($R_0^3 = a^2 b$), one obtains the following equation for the axis ratio, $b/a$:

$$x^3 + 3x^2 + \lambda x + 1 = 0, \tag{5}$$

where $\lambda = 3 - 8(1 + \delta_1 \ell^2 + \delta_2 \ell^4)^3$ and $x = (b/a)^2$. Using Hill–Wheeler parametrization [29], the ellipsoidal deformation can be expressed as $a = R_0 \exp[\sqrt{5/4\pi}\beta \cos(\gamma - 2\pi/3)]$, $b = R_0 \exp[\sqrt{5/4\pi}\beta \cos(\gamma + 2\pi/3)]$, $c = R_0 \exp[\sqrt{5/4\pi}\beta \cos\gamma]$ where $\beta$ and $\gamma$ are the quadrupole deformation and shape parameter, respectively. So, $\beta$ can be expressed as

$$\beta = \frac{2}{3}\left(\frac{4\pi}{5}\right)^{1/2} \ln\left(\frac{b}{a}\right) = 1.057 \ln\left(\frac{b}{a}\right). \tag{6}$$

The values of $b/a$ and $\beta$ extracted for two different sets of 'deformability' parameters (those obtained from RLDM [24] and from fitting CASCADE calculations with the present data) are given in table 2. Typical uncertainty in the estimation of $\beta$ was $\approx$15%. The above results are clearly indicative of the presence of substantial quadrupole deformation in $^{28}$Si* produced through the reaction $^{16}$O + $^{12}$C at all energies, and the deformation is found to increase with increase in spin of the excited composite.

## 4. Discussion

### 4.1 *$\alpha$-Cluster systems and dinuclear orbiting*

All the experimental signatures (energy distributions, angular distributions, $Q$-value etc.) show that the IMFs Li, Be and B emitted from an energy-equilibrated composite form in

**Table 2.** The values of the quadrupole parameters: $A$ – obtained from 'deformability' using RLDM and $B$ – extracted using 'deformability' parameters obtained by fitting the experimental data. The 'deformability' parameters are given in table 1.

| $E_{\rm lab}$ | $(b/a)^A_{\ell_{\rm av}}$ | $\beta^A_{\ell_{\rm av}}$ | $(b/a)^B_{\ell_{\rm av}}$ | $\beta^B_{\ell_{\rm av}}$ |
|---|---|---|---|---|
| 117 | 1.23 | 0.22 | 1.63 | 0.52 |
| 125 | 1.27 | 0.25 | 1.77 | 0.60 |
| 145 | 1.32 | 0.29 | 1.92 | 0.69 |
| 160 | 1.32 | 0.29 | 1.98 | 0.72 |

the reactions involving the $\alpha$-cluster system $^{16}O + {}^{12}C$ for bombarding energies 117, 125, 145 and 160 MeV. So, the total yield should be explained by statistical model calculations. But it has been observed that there is significant enhancement in the yield of the fragment B over the statistical model predictions which suggests additional contribution from other reaction mechanism e.g., dinuclear orbiting. On the contrary, for Li and Be, the binary yields are explained well by CASCADE. This may be due to the fact that, for the case of Li and Be, number of nucleon exchange is more and these are of compound nuclear origin. The energy distributions of the same fragments Li, Be, B have two peaks in the case of other $\alpha$-cluster system $^{12}C + {}^{28}Si$ (and also in non-$\alpha$-cluster systems $^{12}C + {}^{27}Al$ and $^{11}B + {}^{28}Si$). All the experimental signatures confirm that the first peak is originating from equilibrated source and the other from non-equilibrated source. The measured FF fragment yields have been found to be in good agreement with the respective statistical model predictions, EHFM (see figure 9), indicative of the compound nuclear origin of these fragments. However, a previous study on the binary decay of the same system [30] (using inverse kinematical reaction) had reported an enhancement of fragment ($6 \leq Z \leq 8$) yield over the statistical model prediction, thereby conjectured the presence of orbiting mechanism.

One of the important features of dinuclear orbiting is that the number of open channels should be small, which is related to the surface transparency. The calculated NOC for the $\alpha$-cluster system $^{16}O + {}^{12}C$ [11] was compared with neighbouring non-$\alpha$-cluster systems viz., $A = 28, 31$, i.e., ($^{18}O + {}^{10}B$ and $^{19}F + {}^{12}C$ [11]) and it is found that NOCs are much larger (e.g., $\sim 10^4$ times larger) in $^{18}O + {}^{10}B$ and $^{19}F + {}^{12}C$ systems, than those for the $^{16}O + {}^{12}C$ system at all the grazing angular momentum values.

As mentioned earlier, the most important signature of orbiting is the observation of enhanced equilibrium fragment yield near the entrance channel configuration. This enhancement may also be due to the contribution of yield coming from secondary de-excitation of the excited primary heavy fragments. The primary fragments, emitted in the binary reaction, $^{16}O + {}^{12}C$, may have sufficient energy for further decay by emitting lighter fragments, particles and $\gamma$-rays. The yield of these secondary fragments may also contribute to the fragment spectra. To check these, detailed simulations of secondary decay have been performed using the Monte Carlo binary decay version of the statistical decay code LILITA [31] as described in [15]. This result was compared with the difference spectra between total experimental spectra and corresponding fitted Gaussians. It has been found that the difference spectra obtained at 160 MeV are well reproduced by

the secondary decay distributions obtained from LILITA. However, the lower energy tail of the difference spectra obtained at 117 MeV is not fully explained by the secondary decay distributions, which may be due to other additional sources. It is thus evident that the Gaussian fitting procedure for the extraction of primary fragment yield is sufficient to reject the contributions of the secondary decay components, if any, as their energy distributions are different from those of primary fragments [2,32].

Another feature of the orbiting system is that it is usually associated with large deformation. The deformation ($\beta^B_{\ell_{\rm av}}$) of the produced composite, $^{28}$Si$^*$, has been extracted using charged particle spectroscopy as given in table 2. The deformation is found to increase with the spin of the excited composite. The observed deformation in the present study may thus be considered as another indication of orbiting in $^{16}$O + $^{12}$C [16].

### 4.2 *Angular momentum dissipation in DI collision*

It has been observed that the kinetic energy spectra of the fragments (Li, Be and B) emitted in the reactions $^{12}$C + $^{28}$Si, $^{12}$C + $^{27}$Al and $^{11}$B + $^{28}$ Si (typical spectra shown in figure 3) have two peaks. The faster fall off of the fragment angular distribution extracted from the second peak and $Q$-value distributions indicated that this peak is due to DI collision. To understand the variation of the mean kinetic energies of the fragments as well as the energy damping mechanism in general, it is important to study the angular momentum dissipation in DI collision. For light systems, the angular momentum transfer is generally estimated from the total kinetic energy of the rotating dinuclear system, $E_k$, which is given by

$$E_k = V_N(d) + f^2 \frac{\hbar^2 \ell_i(\ell_i + 1)}{2\mu d^2}, \tag{7}$$

where $V_N(d)$ is the contribution from Coulomb and nuclear forces at dinuclear separation distance $d$, $\mu$ is the reduced mass of the dinuclear configuration, $\ell_i$ is the relative angular momentum in the entrance channel and $f$ (final angular momentum $= f\ell_i$) is the numerical factor denoting the fraction of the angular momentum transferred. In the present calculation, the separation distance $d$ between the two fragments has been estimated from the scission point configuration corresponding to the respective asymmetric mass splitting [18], and the corresponding value of kinetic energy is taken as $V_N(d)$. The value of initial angular momentum $\ell_i$ has been taken to be equal to the critical angular momentum for fusion, $\ell_{\rm cr}$. The angular momentum dissipation factors thus obtained are displayed in figure 10 and it is observed that for all the three reactions considered, the experimental values of the mean angular momentum dissipation are more than those predicted under the rolling condition; however, the corresponding sticking limit predictions of $f$ are in fair agreement with the experimental values of the same within the error bar. In all cases, the discrepancy is more for the lighter fragments, and it gradually decreases for the heavier fragments. This may be explained in terms of the following qualitative argument. Microscopically, friction is generated due to stochastic exchange of nucleons between the reacting partners through the window formed by the overlap of the density distributions of the two. Stronger friction essentially means larger degree of density overlap and more nucleon exchange. The lighter DI fragment (corresponds to more net nucleon transfer) originates from deeper collision, for which the interaction time is also

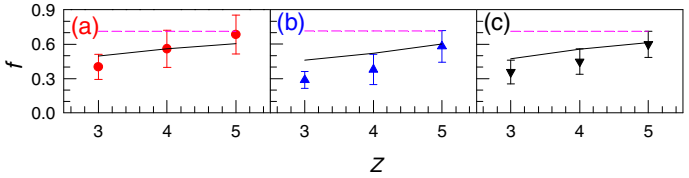


**Figure 10.** The variation of angular momentum dissipation factor $f$ with atomic number of the fragments. The solid circles (red), solid triangles (blue), and inverted triangles (black) are the extracted values of $f$ for (**a**) $^{11}$B + $^{28}$Si, (**b**) $^{12}$C + $^{27}$Al and (**c**) $^{12}$C + $^{28}$Si reactions, respectively. The solid (black) and dotted (pink) curves correspond to the sticking limit and rolling limit predictions for the same, respectively.

larger as seen in figure 5. Therefore, the angular momentum dissipation, originating due to the stochastic nucleon exchange, should also be more, which, at least qualitatively, explains the observed trend.

## 5. Summary

The inclusive double differential cross-sections for IMFs having atomic number, $3 \leq Z \leq 5$, emitted in the reactions involving both $\alpha$-cluster and non-$\alpha$-cluster systems (a) $^{16}$O (117, 125, 145 and 160 MeV) + $^{12}$C and (b) $^{11}$B (64 MeV) + $^{28}$Si, $^{12}$C (73 MeV) + $^{27}$Al and $^{12}$C (77 MeV) + $^{28}$Si, were measured in two separate experiments ((a) and (b)). For system (a), the energy distributions of all fragments at all incident energies were single peaked, having nearly Gaussian shapes with their centroids at the expected kinetic energies corresponding to the binary breakup obtained from the Viola systematics corrected by the corresponding asymmetric factors. The energy distributions of the fragments emitted from the systems (b) were found to have two peaks, one originating from equilibrated source, identified as FF process, and, the other from non-equilibrium source, DI process; each of these peaks was fitted with a separate Gaussian. Characterization of the equilibrium component of fragment spectrum has been done in various ways. $1/\sin\theta_{\text{c.m.}}$ dependence of angular distribution, angle independence of $Q$-value, the nearly equal value of the experimental energy peak and the respective value of the same obtained from Viola systematics suggest that the fragment yield of reaction (a) and yields under the first peak of reactions (b) come from an energy equilibrated composite source. The yields of these fragments were also compared with statistical model calculations. It was observed that there is an enhancement in the yield of B emitted in reaction (a) with respect to both CASCADE and EHFM predictions. The above observation is consistent with the fact that the NOC value for this system is much smaller than those for other two nearby systems – which is indicative of the formation of an orbiting dinuclear complex in $^{16}$O+$^{12}$C at the energies studied here. The enhancement in deformation of $^{28}$S$^{*}$ was also observed from the study of $\alpha$-particle energy spectra. This may be another indication of orbiting in $^{16}$O + $^{12}$C. The total angle-integrated yield of the equilibrium fragments in reactions (b) are in fair agreement with EHFM predictions confirming their compound nuclear origin; even the yields of FF fragments emitted from $\alpha$-cluster system, $^{12}$C + $^{28}$Si, also match with EHFM predictions. It is interesting to note here, that a previous study on

fragment decay from the same system ($^{40}$Ca$^*$, produced through the inverse kinematical reaction $^{28}$Si + $^{12}$C at the same excitation energy [30]) had indicated a possible signature of enhancement in fragment yield (for relatively heavier fragments; $6 \leq Z \leq 8$) over those predicted by the statistical model.

The DI component of the fragment ($3 \leq Z \leq 5$) energy distribution in all the three reactions (b) was studied in detail. It is shown that the DI fragment angular distribution falls off much faster than $1/\sin\theta_{\text{c.m.}}$ distribution. The time-scale of the DI process was estimated from these DI angular distributions. It is observed that for all these reactions, the time-scale, which is related to net nucleon transfer, decreases as the fragment charge increases (closer to the projectile charge). It is also observed that the average $Q$-values for the DI fragments decrease with the increase of emission angle and saturate at higher angles, signifying a saturation in energy damping process beyond these angles. Assuming a compact exit channel configuration (estimated from the extracted FF part of the spectra), the angular momentum dissipation factor, $f$, for the DI process has been extracted. For all the three reactions, the experimental values of $f$ are found to be in fair agreement with the corresponding sticking limit predictions.

## Acknowledgements

The author would like to thank S Bhattacharya, C Bhattacharya, K Banerjee, T K Rana, J K Meena, S Mukhopadhyay, S R Banerjee, A Dey, T K Ghosh, G Mukherjee, D Gupta, R Saha, P Mali, D Pandit, H Pai, Pratap Roy, Suresh Kumar, A Shrivastava, A Chatterjee, P Banerjee, K Ramachandran, K Mahata, S K Pandit and S Santra for their contributions to this work.

## References

[1] S J Sanders, A Szanto de Toledo and C Beck, *Phys. Rep.* **311**, 487 (1999) and references therein
[2] C Bhattacharya *et al*, *Phys. Rev. C* **72**, 021601 (2005)
[3] C Bhattacharya *et al*, *Phys. Rev. C* **69**, 024607 (2004) and references therein
[4] N Carlin Filho *et al*, *Phys. Rev. C* **40**, 91 (1989)
[5] L G Moretto, *Nucl. Phys. A* **247**, 211 (1975)
[6] D Shapira, J L C Ford, J Gomez del Campo, R G Stokstad and R M DeVries, *Phys. Rev. Lett.* **43**, 1781 (1979) and references therein
[7] W Dünnweber *et al*, *Phys. Rev. Lett.* **61**, 927 (1988)
[8] D Shapira *et al*, *Phys. Rev. Lett.* **53**, 1634 (1984)
[9] B Shivakumar, S Ayik, B A Harmon and D Shapira, *Phys. Rev. C* **35**, 1730 (1987)
[10] F Haas and Y Abe, *Phys. Rev. Lett.* **46**, 1667 (1981)
[11] C Beck, Y Abe, N Aissaoui, B Djerroud and F Haas, *Phys. Rev. C* **49**, 2618 (1994) and references therein
[12] M Rousseau *et al*, *Phys. Rev. C* **66**, 034612 (2002)
[13] A Dey *et al*, *Phys. Rev. C* **74**, 044605 (2006)
[14] D Shapira *et al*, *Phys. Rev. Lett.* **53**, 1634 (1984)
[15] S Kundu *et al*, *Phys. Rev. C* **78**, 044601 (2008)
[16] S Kundu *et al*, *Phys. Rev. C* **87**, 024602 (2013)

[17] S Kundu *et al*, *Phys. Rev. C* **85**, 064607 (2012)
[18] C Beck *et al*, *Z. Phys. A* **343**, 309 (1992) and references therein
[19] T Mikumo *et al*, *Phys. Rev. C* **21**, 620 (1980)
[20] F Pühlhofer, *Nucl. Phys. A* **280**, 267 (1977)
[21] T Matsuse, C Beck, R. Nouicer and D Mahboub, *Phys. Rev. C* **55**, 1380 (1997)
[22] S Bhattacharya, K Krishan, S K Samaddar and J N De, *Phys. Rev. C* **37**, 2916 (1988)
[23] M F Vineyard *et al*, *Phys. Rev. C* **47**, 2374 (1993)
[24] S Cohen, F Plasil and W J Swiatecki, *Ann. Phys.* **82**, 557 (1974)
[25] J R Huizenga, A N Behkami, I M Govil, W U Schröder and J Tõke, *Phys. Rev. C* **40**, 668 (1989)
[26] D Mahboub *et al*, *Phys. Rev. C* **69**, 034616 (2004)
[27] C Bhattacharya *et al*, *Phys. Rev. C* **69**, 024607 (2004)
[28] M Rousseau *et al*, *Phys. Rev. C* **66**, 034612 (2002)
[29] D L Hill and J A Wheeler, *Phys. Rev.* **89**, 1102 (1953)
[30] D Shapira *et al*, *Phys. Lett. B* **114**, 111 (1982)
[31] J Gomez del Campo and R G Stokstad, Description and use of the Monte Carlo code "LILITA", *Tech. Rep. ORNL-TM 7295*, Oak Ridge National Laboratory, TN, USA (1981)
[32] A Dey *et al*, *Phys. Rev. C* **76**, 034608 (2007) and references therein